Nucleon-nucleon *t*-matrix interaction for scattering at intermediate energies

M. A. Franey
Department of Physics, University of Minnesota, Minneapolis, Minnesota 55455

W. G. Love
Department of Physics and Astronomy, University of Georgia, Athens, Georgia 30602
and Los Alamos Scientific Laboratory, Los Alamos, New Mexico 87545
(Received 9 October 1984)

A local nucleon-nucleon effective interaction based on current phenomenological nucleon-nucleon scattering amplitudes has been constructed at several bombarding energies between 50 and 1000 MeV/nucleon within a dynamically nonrelativistic framework. The form of the interaction has been chosen for convenience in performing nucleon-nucleus scattering calculations in this energy range and for ease of comparison with one-boson-exchange potential models. Some properties of this interaction are compared with those of an earlier version based on an older set of nucleon-nucleon amplitudes.

I. INTRODUCTION

The study of proton elastic and inelastic scattering at intermediate energies continues to provide information on nuclear structure which is either complementary or comparative to that obtained with other probes.[1–10] Such studies usually employ the single-scattering approximation (SSA) which has met with varying degrees of success. For certain types of transitions, corrections to the SSA based on the free nucleon-nucleon (NN) t matrix are known to be important. To date, the two most important of these have been identified as (1) medium modifications[7,8] due to Pauli blocking and short-range correlations, and (2) the use of a relativistic (Dirac) framework.[9,11] In both cases it is useful and instructive to determine clearly the departure from the nonrelativistic free t-matrix approach. Indeed, a complete implementation of the relativistic framework will require much more careful consideration of the nuclear structure which may be extracted from (or input to) calculations of nucleon-nucleus scattering. Where corrections to the nonrelativistic free t-matrix approach are relatively small, as appears to be the case for the excitation of Gamow-Teller[2] and high-spin[4] states of unnatural parity, for example, this approach has the advantage of simplicity and familiarity. To properly assess the relative merits of the various approaches clearly requires the most accurate available description of the NN amplitudes.

The purpose of this paper is primarily to update the effective interaction presented in Ref. 5 which is based on NN amplitudes determined before or during 1980. The present interaction is based on the SP84 amplitudes of Arndt[12] and incorporates considerably more NN data at intermediate energies than those amplitudes used earlier.[5] In particular, the data base used to determine the SP84 amplitudes contain 96% (28%) more pp (np) data points than does the data base used to determine the CK80 amplitudes used in Ref. 5. A large part of this increase reflects the measurement of NN spin observables which are especially sensitive to the spin-dependent amplitudes.

The basic notation and techniques used here are the same as in the parent paper (Ref. 5) so that we describe primarily the extensions to that work.

II. THE EFFECTIVE INTERACTION

In Ref. 5, the free NN scattering amplitudes $M(E_{\mathrm{c.m.}},\theta)$ expressed by

$$M(E_{\mathrm{c.m.}},\theta)=A+B\boldsymbol{\sigma}_1\cdot\hat{\mathbf{n}}\boldsymbol{\sigma}_2\cdot\hat{\mathbf{n}}+C(\boldsymbol{\sigma}_1+\boldsymbol{\sigma}_2)\cdot\hat{\mathbf{n}}+E\boldsymbol{\sigma}_1\cdot\hat{\mathbf{q}}\boldsymbol{\sigma}_2\cdot\hat{\mathbf{q}}+F\boldsymbol{\sigma}_1\cdot\hat{\mathbf{Q}}\boldsymbol{\sigma}_2\cdot\hat{\mathbf{Q}} \quad (1)$$

were constructed from the phase shift sets given in Table I of Ref. 5. In this work the NN amplitudes have been obtained from the Los Alamos Meson Physics Facility (LAMPF) version of the scattering analysis interactive dial-in (SAID) program[12] of Arndt and Roper. With the exception of the 270 MeV t matrix, the amplitudes used herein are from the data set SP84 dated January 23, 1984. At 270 MeV the SP84 amplitudes dated April 19, 1984 were used. The "NP1" and "NP" subsets[12] were used with all electromagnetic and charge-dependent effects suppressed. In Ref. 5 the phases at some energies were obtained from the work of Arndt and Roper; at other energies they were obtained from Ref. 13.

As in Ref. 5, we represent the effective interaction V_{12} in each NN channel by a sum of central (C), spin-orbit (LS), and tensor (T) terms:

$$V_{12}=V^{C}(r_{12})+V^{LS}(r_{12})\mathbf{L}\cdot\mathbf{S}+V^{T}(r_{12})S_{12}\ , \quad (2)$$

each part of which is a superposition of Yukawa terms or r^2x Yukawa terms for the tensor parts. In particular

$$V^{C}(r)=\sum_{i=1}^{N_C}V_i^{C}Y(r/R_i),\quad Y(x)=e^{-x}/x\ , \quad (3a)$$

$$V^{LS}(r)=\sum_{i=1}^{N_{LS}}V_i^{LS}Y(r/R_i)\ , \quad (3b)$$

TABLE I. Nucleon-nucleon t-matrix interaction strengths in the nucleon-nucleon c.m. system derived from the LAMPF version of SP84 amplitudes (Ref. 12) dated January 23, 1984. (At 270 MeV, the SP84 amplitudes dated April 19, 1984 were used.) The TNE and TNO strengths are in MeV fm^{-2}; all others are in MeV. The ranges are in fm; $NE\pm n$ denotes $N\times 10^{\pm n}$.

t-matrix interaction strengths at 50 MeV

	Real					Imag			
Range	SE	TE	SO	TO	Range	SE	TE	SO	TO
0.25	1.34417E+04	1.77164E+04	−1.13818E+05	4.64708E+03	0.25	−7.38213E+02	1.15584E+04	1.74344E+04	8.98647E+03
0.40	−3.89887E+03	−4.96816E+03	1.23150E+04	−1.42516E+03	0.40	−2.12695E+02	−3.87153E+03	−2.27828E+03	−1.38108E+03
1.40	−1.05000E+01	−1.05000E+01	3.15000E+01	3.50000E+00	1.40				
Range	LSE	LSO	TNE	TNO	Range	LSE	LSO	TNE	TNO
0.25	−2.19622E+04	4.47808E+03	1.71786E+05	2.68030E+03	0.25	−8.84002E+04	−3.52978E+03	1.72442E+04	−5.07468E+03
0.40	−1.01819E+03	−1.30427E+03	−1.88801E+04	−6.36557E+01	0.40	5.54246E+03	5.64196E+02	−1.67281E+03	4.66389E+02
0.55			2.44410E+03	−5.19215E+00	0.55			1.31469E+02	−3.52030E+01
0.70			−2.80717E+02	2.49188E+01	0.70			−6.16547E+00	2.06097E+00

t-matrix interaction strengths at 100 MeV

	Real					Imag			
Range	SE	TE	SO	TO	Range	SE	TE	SO	TO
0.25	1.05984E+04	8.89417E+03	−1.82269E+04	7.69888E+03	0.25	6.45678E+02	1.13187E+04	7.34567E+03	2.41839E+03
0.40	−3.21264E+03	−2.79683E+03	2.53674E+03	−1.60906E+03	0.40	−3.43385E+02	−3.62479E+03	−1.40826E+03	−6.83690E+02
1.40	−1.05000E+01	−1.05000E+01	3.15000E+01	3.50000E+00	1.40				
Range	LSE	LSO	TNE	TNO	Range	LSE	LSO	TNE	TNO
0.25	−1.14015E+04	−1.68570E+03	6.89650E+04	9.03713E+02	0.25	−1.95620E+04	−1.54304E+03	1.72934E+04	−8.43141E+03
0.40	−5.97390E+02	−6.14658E+02	−1.02174E+04	8.09495E+01	0.40	2.18728E+03	2.41376E+02	−2.55965E+03	1.12487E+03
0.55			1.64327E+03	−3.15586E+00	0.55			3.49963E+02	−1.55646E+02
0.70			−2.32416E+02	2.14986E+01	0.70			−3.03573E+01	1.41551E+01

t-matrix interaction strengths at 140 MeV

	Real					Imag			
Range	SE	TE	SO	TO	Range	SE	TE	SO	TO
0.25	9.47399E+03	5.95751E+03	−2.54198E+03	7.86482E+03	0.25	1.12801E+03	9.74299E+03	2.87199E+03	4.68991E+02
0.40	−2.92063E+03	−1.97848E+03	7.82429E+02	−1.56881E+03	0.40	−4.06183E+02	−3.13550E+03	−9.83301E+02	−4.40472E+02
1.40	−1.05000E+01	−1.05000E+01	3.15000E+01	3.50000E+00	1.40				
Range	LSE	LSO	TNE	TNO	Range	LSE	LSO	TNE	TNO
0.25	−7.54122E+03	−3.09627E+03	3.84343E+04	1.65808E+03	0.25	−7.25238E+03	−9.73518E+02	1.39275E+04	−8.64691E+03
0.40	−4.64320E+02	−3.94780E+02	−6.94577E+03	−1.18309E+02	0.40	1.31936E+03	1.41641E+02	−2.54752E+03	1.35798E+03
0.55			1.25503E+03	4.66086E+01	0.55			4.22819E+02	−2.25213E+02
0.70			−2.02390E+02	1.40732E+01	0.70			−4.27937E+01	2.33058E+01

TABLE I. (*Continued*).

t-matrix interaction strengths at 175 MeV

	Real					Imag			
Range	SE	TE	SO	TO	Range	SE	TE	SO	TO
0.25	8.84575E+03	4.50223E+03	2.57057E+03	7.64504E+03	0.25	1.35124E+03	8.48148E+03	5.38800E+02	−4.65650E+02
0.40	−2.74630E+03	−1.53068E+03	1.31554E+02	−1.50695E+03	0.40	−4.44157E+02	−2.75204E+03	−7.37824E+02	−3.10545E+02
1.40	−1.05000E+01	−1.05000E+01	3.15000E+01	3.50000E+00	1.40				
Range	LSE	LSO	TNE	TNO	Range	LSE	LSO	TNE	TNO
0.25	−5.54835E+03	−3.58318E+03	2.35229E+04	1.54653E+03	0.25	−3.33593E+03	−6.09087E+02	1.12392E+04	−8.33357E+03
0.40	−3.98098E+02	−2.88049E+02	−4.96930E+03	−1.35162E+02	0.40	9.43863E+02	8.99986E+01	−2.34963E+03	1.44887E+03
0.55			9.60072E+02	5.59220E+01	0.55			4.35747E+02	−2.65783E+02
0.70			−1.74041E+02	1.17774E+01	0.70			−4.78589E+01	2.95019E+01

t-matrix interaction strengths at 210 MeV

	Real					Imag			
Range	SE	TE	SO	TO	Range	SE	TE	SO	TO
0.25	8.39519E+03	3.56735E+03	4.71412E+03	7.31342E+03	0.25	1.45853E+03	7.41973E+03	−9.19824E+02	−1.07689E+03
0.40	−2.61566E+03	−1.21675E+03	−1.93752E+02	−1.43949E+03	0.40	−4.69589E+02	−2.43121E+03	−5.63008E+02	−2.17827E+02
1.40	−1.05000E+01	−1.05000E+01	3.15000E+01	3.50000E+00	1.40				
Range	LSE	LSO	TNE	TNO	Range	LSE	LSO	TNE	TNO
0.15			3.25631E+05	5.09043E+04	0.15			2.12453E+05	−1.47371E+05
0.25	−4.27719E+03	−3.75475E+03	−2.47288E+04	−4.09914E+03	0.25	−1.59970E+03	−2.85062E+02	−1.58050E+04	9.39215E+03
0.40	−3.51873E+02	−2.23300E+02	6.54904E+02	3.34910E+02	0.40	7.22578E+02	5.25282E+01	4.78422E+02	−3.03689E+02
0.70			−6.97061E+01	1.48573E+01	0.70			−4.70474E+00	3.33699E+00

t-matrix interaction strengths at 270 MeV

	Real					Imag			
Range	SE	TE	SO	TO	Range	SE	TE	SO	TO
0.25	5.89037E+03	3.47090E+03	−5.15172E+04	5.80993E+03	0.25	2.21264E+03	3.62968E+03	−2.20625E+03	−2.86675E+03
0.40	−1.36195E+03	−1.34793E+03	1.67780E+04	−1.03573E+03	0.40	−9.00238E+02	−6.76925E+02	−3.51375E+02	2.28178E+02
0.55	−2.29750E+02	1.04810E+02	−2.59918E+03	−5.07069E+01	0.55	8.59426E+01	−2.79248E+02	−6.27354E+00	−5.01090E+01
1.40	−1.05000E+01	−1.05000E+01	3.15000E+01	3.50000E+00	1.40				
Range	LSE	LSO	TNE	TNO	Range	LSE	LSO	TNE	TNO
0.15			8.05275E+04	1.56052E+04	0.15			1.27002E+05	−1.08413E+05
0.25	−6.99955E+03	−3.32120E+03	−7.43299E+03	−1.09107E+03	0.25	−8.07467E+02	4.24916E+02	−1.04694E+04	7.47658E+03
0.40	3.49040E+02	−2.94795E+02	−2.95714E+01	1.77657E+02	0.40	5.59786E+02	−6.12376E+01	3.85365E+02	−2.84082E+02
0.55	−6.89521E+01	2.23046E+01			0.55	−4.87654E+00	9.69778E+00		
0.70			−6.02151E+01	1.61522E+01	0.70			−4.85957E+00	3.72577E+00

TABLE I. (*Continued*).

t-matrix interaction strengths at 325 MeV

	Real					Imag			
Range	SE	TE	SO	TO	Range	SE	TE	SO	TO
0.25	5.756 64E+03	2.665 32E+03	−2.909 46E+04	5.064 49E+03	0.25	2.332 38E+03	3.035 12E+03	−3.428 69E+03	−3.113 20E+03
0.40	−1.348 84E+03	−1.001 77E+03	1.085 10E+04	−8.887 19E+02	0.40	−1.019 15E+03	−5.479 07E+02	−3.925 45E+01	2.938 04E+02
0.55	−2.162 26E+02	8.512 26E+01	−1.839 54E+03	−5.565 69E+01	0.55	1.097 47E+02	−2.566 26E+02	−3.312 54E+01	−5.327 25E+01
1.40	−1.050 00E+01	−1.050 00E+01	3.150 00E+01	3.500 00E+00	1.40				
Range	LSE	LSO	TNE	TNO	Range	LSE	LSO	TNE	TNO
0.15			−6.104 15E+03	7.319 66E+03	0.15			7.846 40E+04	−8.383 23E+04
0.25	−4.707 87E+03	−3.272 10E+03	−3.595 61E+02	−3.197 66E+02	0.25	−5.456 00E+02	8.862 39E+02	−6.669 60E+03	6.120 59E+03
0.40	1.785 49E+02	−2.150 65E+02	−3.713 69E+02	1.211 90E+02	0.40	4.886 96E+02	−1.262 02E+02	2.786 89E+02	−2.599 93E+02
0.55	−5.357 70E+01	1.189 46E+01			0.55	−1.107 17E+01	1.491 79E+01		
0.70			−5.398 99E+01	1.644 27E+01	0.70			−4.214 45E+00	3.808 85E+00

t-matrix interaction strengths at 425 MeV

	Real					Imag			
Range	SE	TE	SO	TO	Range	SE	TE	SO	TO
0.25	5.512 14E+03	1.409 19E+03	−1.070 26E+04	4.224 21E+03	0.25	3.492 27E+03	2.027 74E+03	−4.193 02E+03	−3.367 21E+03
0.40	−1.296 66E+03	−3.648 23E+02	5.123 68E+03	−7.424 32E+02	0.40	−1.763 95E+03	−2.634 65E+02	3.121 40E+02	3.801 06E+02
0.55	−2.021 24E+02	1.211 37E+01	−9.726 63E+02	−5.962 91E+01	0.55	2.344 61E+02	−2.516 87E+02	−7.698 47E+01	−6.131 74E+01
1.40	−1.050 00E+01	−1.050 00E+01	3.150 00E+01	3.500 00E+00	1.40				
Range	LSE	LSO	TNE	TNO	Range	LSE	LSO	TNE	TNO
0.15			−3.017 82E+04	−6.931 96E+03	0.15			3.693 47E+04	−5.569 98E+04
0.25	−2.775 81E+03	−2.742 84E+03	1.279 83E+03	1.152 28E+03	0.25	−3.826 11E+02	1.586 60E+03	−1.800 84E+03	3.765 58E+03
0.40	2.952 74E+01	−2.062 20E+02	−4.487 51E+02	−1.142 21E+01	0.40	4.100 99E+02	−2.388 14E+02	4.409 81E+01	−1.495 71E+02
0.55	−3.480 21E+01	1.148 75E+01			0.55	−1.739 62E+01	2.677 98E+01		
0.70			−5.112 01E+01	1.824 45E+01	0.70			−6.544 21E−01	2.034 86E+00

t-matrix interaction strengths at 515 MeV

	Real					Imag			
Range	SE	TE	SO	TO	Range	SE	TE	SO	TO
0.25	4.116 80E+03	5.209 97E+02	−1.991 45E+03	3.858 87E+03	0.25	5.522 80E+03	1.331 19E+03	−4.530 95E+03	−3.027 81E+03
0.40	−6.541 60E+02	1.321 11E+02	1.792 98E+03	−6.949 43E+02	0.40	−2.953 26E+03	−4.763 19E+01	6.069 59E+02	2.766 10E+02
0.55	−2.857 79E+02	−5.919 71E+01	−3.710 19E+02	−5.864 96E+01	0.55	4.375 28E+02	−2.596 86E+02	−1.284 15E+02	−5.919 77E+01
1.40	−1.050 00E+01	−1.050 00E+01	3.150 00E+01	3.500 00E+00	1.40				
Range	LSE	LSO	TNE	TNO	Range	LSE	LSO	TNE	TNO
0.11			−1.960 83E+06	−1.383 26E+05	0.11			−2.030 86E+05	−4.848 77E+05
0.15			4.448 01E+05	2.678 66E+04	0.15			6.987 80E+04	8.079 24E+04
0.25	−1.868 50E+03	−2.105 24E+03	−1.319 09E+04	−1.616 38E+02	0.25	−2.294 41E+02	2.122 28E+03	−1.260 88E+03	−1.254 18E+03
0.40	−5.891 49E+01	−2.647 73E+02			0.40	3.546 67E+02	−3.160 13E+02		
0.55	−2.092 89E+01	1.989 62E+01			0.55	−1.959 60E+01	3.652 58E+01		
0.70			−5.459 07E+01	1.804 32E+01	0.70			−4.881 06E−02	3.692 80E−01

TABLE I. (*Continued*).

t-matrix interaction strengths at 650 MeV

	Real					Imag			
Range	SE	TE	SO	TO	Range	SE	TE	SO	TO
0.15	−3.921 78E +04	−1.139 60E +04	1.094 28E +05	−3.700 87E +04	0.15	2.560 17E +04	−1.794 89E +04	−5.360 21E +04	−1.656 74E +04
0.25	1.999 51E +04	5.129 98E +03	−2.160 72E +04	1.218 68E +04	0.25	−7.830 54E +03	9.733 18E +03	9.005 82E +03	3.104 62E +03
0.40	−2.833 62E +03	−3.991 20E +02	1.706 30E +03	−1.513 48E +03	0.40	−9.478 53E +01	−1.758 96E +03	−8.671 57E +02	−7.973 27E +02
1.40	−1.050 00E +01	−1.050 00E +01	3.150 00E +01	3.500 00E +00	1.40				
Range	LSE	LSO	TNE	TNO	Range	LSE	LSO	TNE	TNO
0.11			−1.930 88E +06	−4.207 33E +05	0.11			−4.388 55E +05	−7.692 79E +05
0.15	−1.040 85E +04	1.036 98E +04	4.517 25E +05	9.499 69E +04	0.15	−2.510 57E +04	9.192 89E +03	1.311 17E +05	1.706 80E +05
0.25	5.992 48E +01	−3.690 62E +03	−1.372 86E +04	−2.346 50E +03	0.25	3.033 30E +03	−1.241 65E +02	−2.510 54E +03	−4.734 66E +03
0.40	−2.229 63E +02	−5.501 26E +01			0.40	5.478 08E +01	2.290 30E +01		
0.70			−5.202 53E +01	1.830 95E +01	0.70			3.976 20E −01	1.230 98E +00

t-matrix interaction strengths at 725 MeV

	Real					Imag			
Range	SE	TE	SO	TO	Range	SE	TE	SO	TO
0.15	−4.242 81E +04	−1.161 86E +04	1.538 33E +05	−7.729 34E +04	0.15	1.333 43E +04	−1.753 04E +04	−5.796 52E +04	−2.803 78E +02
0.25	2.103 58E +04	5.085 07E +03	−3.326 64E +04	2.060 31E +04	0.25	−3.197 46E +03	9.503 88E +03	1.090 94E +04	6.914 32E +02
0.40	−2.828 53E +03	−3.233 52E +02	2.754 86E +03	−2.029 64E +03	0.40	−5.407 02E +02	−1.733 38E +03	−1.055 59E +03	−8.532 13E +02
1.40	−1.050 00E +01	−1.050 00E +01	3.150 00E +01	3.500 00E +00	1.40				
Range	LSE	LSO	TNE	TNO	Range	LSE	LSO	TNE	TNO
0.11			−1.857 65E +06	−5.175 44E +05	0.11			−4.836 93E +05	−8.008 60E +05
0.15	−2.466 25E +02	1.659 23E +04	4.402 70E +05	1.218 05E +05	0.15	−2.127 65E +04	5.335 84E +03	1.485 28E +05	1.877 41E +05
0.25	−8.892 80E +02	−4.531 26E +03	−1.357 80E +04	−3.040 31E +03	0.25	2.830 36E +03	5.968 61E +02	−3.124 98E +03	−6.019 44E +03
0.40	−1.700 52E +02	1.735 17E +00			0.40	3.790 15E +01	−1.132 19E +01		
0.70			−5.077 14E +01	1.809 46E +01	0.70			7.423 36E −01	1.977 37E +00

t-matrix interaction strengths at 800 MeV

	Real					Imag			
Range	SE	TE	SO	TO	Range	SE	TE	SO	TO
0.15	−4.269 64E +04	−1.161 95E +04	1.748 21E +05	−1.092 47E +05	0.15	2.855 32E +03	−1.616 42E +04	−6.184 52E +04	9.231 41E +03
0.25	2.108 09E +04	4.962 25E +03	−4.026 15E +04	2.753 71E +04	0.25	1.024 43E +03	8.880 72E +03	1.277 74E +04	−1.273 55E +03
0.40	−2.776 79E +03	−2.468 93E +02	3.512 29E +03	−2.428 34E +03	0.40	−9.962 33E +02	−1.665 54E +03	−1.260 88E +03	−7.835 07E +02
1.40	−1.050 00E +01	−1.050 00E +01	3.150 00E +01	3.500 00E +00	1.40				
Range	LSE	LSO	TNE	TNO	Range	LSE	LSO	TNE	TNO
0.11			−1.743 54E +06	−5.846 29E +05	0.11			−4.311 98E +05	−8.213 21E +05
0.15	6.214 87E +03	2.202 54E +04	4.195 42E +05	1.401 07E +05	0.15	−1.720 13E +04	3.198 57E +03	1.443 84E +05	1.958 52E +05
0.25	−1.564 93E +03	−5.309 93E +03	−1.321 87E +04	−3.320 28E +03	0.25	2.563 70E +03	1.047 71E +03	−3.356 44E +03	−6.586 79E +03
0.40	−1.265 89E +02	5.534 15E +01			0.40	2.710 88E +01	−4.512 99E +01		
0.70			−4.967 24E +01	1.785 68E +01	0.70			1.082 16E +00	2.814 77E +00

TABLE I. (*Continued*).

t-matrix interaction strengths at 1000 MeV

Real					Imag				
Range	SE	TE	SO	TO	Range	SE	TE	SO	TO
0.15	$-3.97083E+04$	$-1.30391E+04$	$1.77348E+05$	$-1.30837E+05$	0.15	$-1.41428E+04$	$-1.10215E+04$	$-6.87148E+04$	$8.44559E+03$
0.25	$1.98196E+04$	$5.44155E+03$	$-4.64711E+04$	$3.36377E+04$	0.25	$8.67176E+03$	$6.49075E+03$	$1.70941E+04$	$-2.02912E+03$
0.40	$-2.56051E+03$	$-1.99668E+02$	$4.59027E+03$	$-2.80368E+03$	0.40	$-1.99888E+03$	$-1.38744E+03$	$-1.82287E+03$	$-6.45713E+02$
1.40	$-1.05000E+01$	$-1.05000E+01$	$3.15000E+01$	$3.50000E+00$	1.40				
Range	LSE	LSO	TNE	TNO	Range	LSE	LSO	TNE	TNO
0.11			$-1.73721E+06$	$-5.18921E+05$	0.11			$-3.12921E+05$	$-3.90684E+05$
0.15	$1.25797E+04$	$2.72900E+04$	$4.34929E+05$	$1.33075E+05$	0.15	$-7.66320E+03$	$1.89246E+03$	$1.20438E+05$	$9.01634E+04$
0.25	$-2.41149E+03$	$-6.00841E+03$	$-1.39942E+04$	$-3.33354E+03$	0.25	$1.79314E+03$	$1.31492E+03$	$-3.11610E+03$	$-3.81076E+03$
0.40	$-4.58047E+01$	$1.38283E+02$			0.40	$1.57346E+01$	$-9.24643E+01$		
0.70			$-4.57834E+01$	$1.76171E+01$	0.70			$1.36250E+00$	$1.82222E+00$

$$V^T(r)=\sum_{i=1}^{N_T} V_i^T r^2 Y(r/R_i) , \qquad (3c)$$

where the V's are complex strengths which are adjusted, as described in Ref. 5, until the antisymmetrized momentum-space matrix elements of V_{12} reproduce the on-shell NN t matrix; the ranges R_i were chosen as described in Ref. 5. For the tensor amplitudes a region of momentum transfer bounded by q_1 and q_2 was excluded from the fitting for reasons described in Ref. 5. For the common energies, q_1 and q_2 were taken to be the same as in Ref. 5; at 725 MeV $q_1=3.75$, $q_2=5.80$; at 1000 MeV $q_1=4.00$, $q_2=6.90$, where all q's are in fm^{-1}.

Table I lists the parameters of the new NN interaction at each energy; namely, the complex strengths for each Yukawa of designated range. For use in nucleon-nucleus calculations, these strengths require a common kinematic factor described by Eq. (19) of Ref. 5.

In order to illustrate a few of the many implications of the interaction in Table I for calculations of nucleon-nucleus scattering it is useful to plot or tabulate some of its important composite characteristics.

For consideration of scattering at small momentum transfers where the central part of the t matrix usually[5] dominates, it is convenient to know the strength of the t matrix near $q=0$. Table II contains the moduli (R) and phases (ϕ) of $t^c(q=0)=Re^{i\phi}$ as a function of the projectile nucleon's laboratory kinetic energy (T_{lab}) for each spin and isospin transfer combination $(0,\sigma,\tau,\sigma\tau)$. Both direct and exchange terms[5] are included in the tabulated quantities. A plot of these moduli vs T_{lab} is qualitatively similar to that shown in Ref. 5 and is therefore not shown. The nearly real nature of $t_{\sigma\tau}$, which is believed to be mediated by the one-pion exchange potential (OPEP), is apparent at all energies considered. Similarly, the nearly imaginary nature of t_τ below $\sim$200 MeV and t_0 above $\sim$500 MeV is evident. The phases in Table II are useful for calculating $t^c(q=0)$ in other forms such as in the neutron-proton representation.

There has been considerable interest[14] recently in extracting neutron transition densities or neutron transition matrix elements by combining studies of hadron and electron scattering. In the case of inelastic nucleon scattering this requires a knowledge of the coupling between like and unlike nucleons at the relevant energy. When only transition matrix elements are extracted, the values of $t_{\text{pp}}^c(q=0)$ and $t_{\text{pn}}^c(q=0)$ are typically used. Figure 1 shows a plot of the moduli (volume integrals) and rms radii of the spin-independent ($\Delta S=0$) and spin-dependent ($\Delta S=1$) parts of t_{pp}^c and t_{pn}^c between 50 and 1000 MeV. The rms radii here are defined by $\langle r^2\rangle^{1/2}=|J_2/J_0|^{1/2}$, where

$$J_0=t^c(q=0)=4\pi\int_0^\infty r^2 t^c(r)dr ,$$
$$J_2=-6\left[\frac{\partial t^c}{\partial q^2}\right]_{q=0}=4\pi\int_0^\infty r^4 t^c(r)dr . \qquad (4)$$

The much larger $\langle r^2\rangle^{1/2}$ for the spin-dependent parts of the force may be traced largely to the contribution of the OPEP which has an rms radius of $\sim$3.5 fm. Both direct and approximate-exchange[5] terms are included in t^c.

TABLE II. Moduli and phases of the central parts of the t-matrix interaction in Table I at $q=0$ as a function of projectile energy ($T_{\rm lab}$). The moduli (R) are in MeV fm^3; the phases (ϕ) are in deg. The exchange terms were included as described in Ref. 5.

$T_{\rm lab}$	(R_0,ϕ_0)	(R_σ,ϕ_σ)	(R_τ,ϕ_τ)	$(R_{\sigma\tau},\phi_{\sigma\tau})$
50	494.6,227.9	60.0,24.5	170.4,78.7	178.2,33.3
100	379.6,219.4	16.4,295.4	95.7,75.5	162.6,12.5
140	324.9,220.8	24.7,255.8	69.2,83.9	160.1,4.2
175	291.5,224.9	27.4,249.0	56.8,95.4	157.9,359.7
210	269.6,230.2	26.5,248.8	50.5,108.3	155.5,356.9
270	257.5,238.4	22.6,272.5	48.9,126.1	147.8,354.3
325	253.9,245.6	20.0,293.2	50.6,139.5	144.2,353.4
425	274.5,254.9	15.4,352.5	57.4,160.5	138.4,354.9
515	316.7,261.5	16.1,35.2	64.2,178.2	133.3,357.0
650	409.4,269.0	9.7,184.6	80.6,198.9	127.8,356.5
725	450.6,271.2	21.7,204.5	92.7,204.0	126.0,356.1
800	477.9,273.3	27.3,205.4	101.5,206.3	125.5,356.3
1000	523.4,278.2	29.3,186.8	112.5,209.6	125.4,358.5

A quantity which has been particularly useful[2] in the identification and interpretation of isovector excitations, in general, and charge exchange excitations, in particular, is the ratio $|t_{\sigma\tau}/t_\tau|^2$ at $q=0$. The energy dependence of this quantity is shown in Fig. 2 for the present free interaction as well as for the interaction published[5] previously using older phase shifts (79 phases) obtained by different authors.[5] The newer interaction is smoother than the older one and is in better agreement[15] with experiment near 200 MeV. The experimental values[15] are denoted by triangles.

One of the distinguishing features[1,16,17] of the (p,p′) reaction for exciting unnatural parity states is its sensitivity to both the longitudinal and transverse spin densities. By comparison, the (π,π') and (e,e′) reactions sample only the transverse components of the spin densities. Recent advances[17] in the measurement and interpretation of selected spin observables in inelastic proton scattering permit an approximate separation of these two types of transition densities. The sensitivity of nucleon scattering to each of these densities depends on the relative strengths of the longitudinal and transverse NN coupling. We denote these couplings[16] by $V^l(q)$ and $V^t(q)$, respectively, where for each isospin transfer,

$$V^l(q)=t_1^C(q)-2t^T(q)\ , \tag{5a}$$

$$V^t(q)=t_1^C(q)+t^T(q)\ , \tag{5b}$$

and

$$\begin{aligned} t_1^C(q)&=\tilde{V}_D^C(q)+\tilde{V}_E^C(k_A)\ ,\\ t^T(q)&=\tilde{V}_D^T(q)-\tfrac{1}{2}\tilde{V}_E^T(k_A)\ . \end{aligned} \tag{5c}$$

Here $\tilde{V}_D^{C,T}$ are the Fourier transforms of the central and tensor parts of the force given by Eq. (2); $\tilde{V}_E^{C,T}$ denote the exchange contributions and are given by the Fourier transforms[5] of the central and tensor parts of the force in

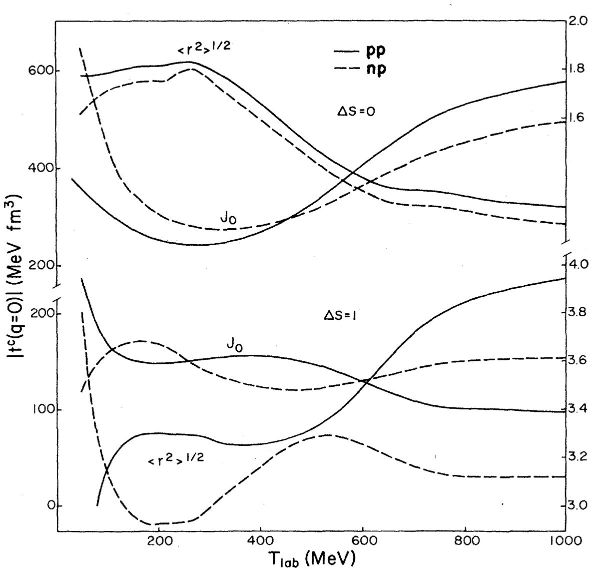

FIG. 1. Volume integrals (J_0) and rms radii [see Eq. (4)] of the central parts of the present effective interaction in a neutron-proton representation as a function of nucleon kinetic energy. pp (np) denotes the proton-proton (neutron-proton) part of the interaction.

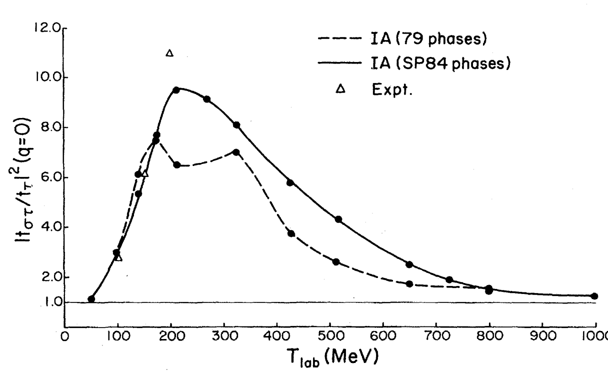

FIG. 2. Energy dependence of the ratio $|t_{\sigma\tau}(q=0)/t_\tau(q=0)|^2$.

Eq. (2), with the signs of the odd-state parts of V_{12} reversed.[18] The subscript 1 on t_1^C denotes that part of $V_{D,E}^C$ proportional to $\sigma_1 \cdot \sigma_2$; k_A is the magnitude of the nucleon-nucleus relative asymptotic momentum. Figure 3 shows the moduli of the isoscalar ($\Delta T = 0$) and isovector ($\Delta T = 1$) components of the longitudinal and transverse NN couplings as a function of momentum transfer (q) at selected projectile energies. Both longitudinal and transverse isovector couplings are seen to vary with energy in a rather smooth way. At a microscopic level this is presumably due to the stabilizing influence of the one-pion and one-rho meson exchange terms,[16] respectively, in the isovector "channel." These particular meson exchanges contribute to the isoscalar parts of the interaction only through antisymmetrization, and in the isoscalar channel the energy dependence of the longitudinal and transverse parts of the force is not nearly as smooth as in the isovector channel.

The most conspicuous feature of the isovector couplings is the strong interference between the central and tensor contributions to the longitudinal term in the interval between $q = 0.5$ and $1.0\ \text{fm}^{-1}$. This results in the isovector transverse coupling being considerably larger than the longitudinal coupling in this important regime of momentum transfer and may make it relatively difficult to identify isovector longitudinal spin modes at these momentum transfers without making rather selective measurements.[17] Figure 4 shows the moduli of the ratio of transverse to longitudinal couplings at $T_{\text{lab}} = 140$ and 425 MeV. For the isovector parts of the force, the curves are qualitatively similar at the two energies and show explicitly the transverse (longitudinal) dominance at small (large) momentum transfer. This suggests that for isovector spin

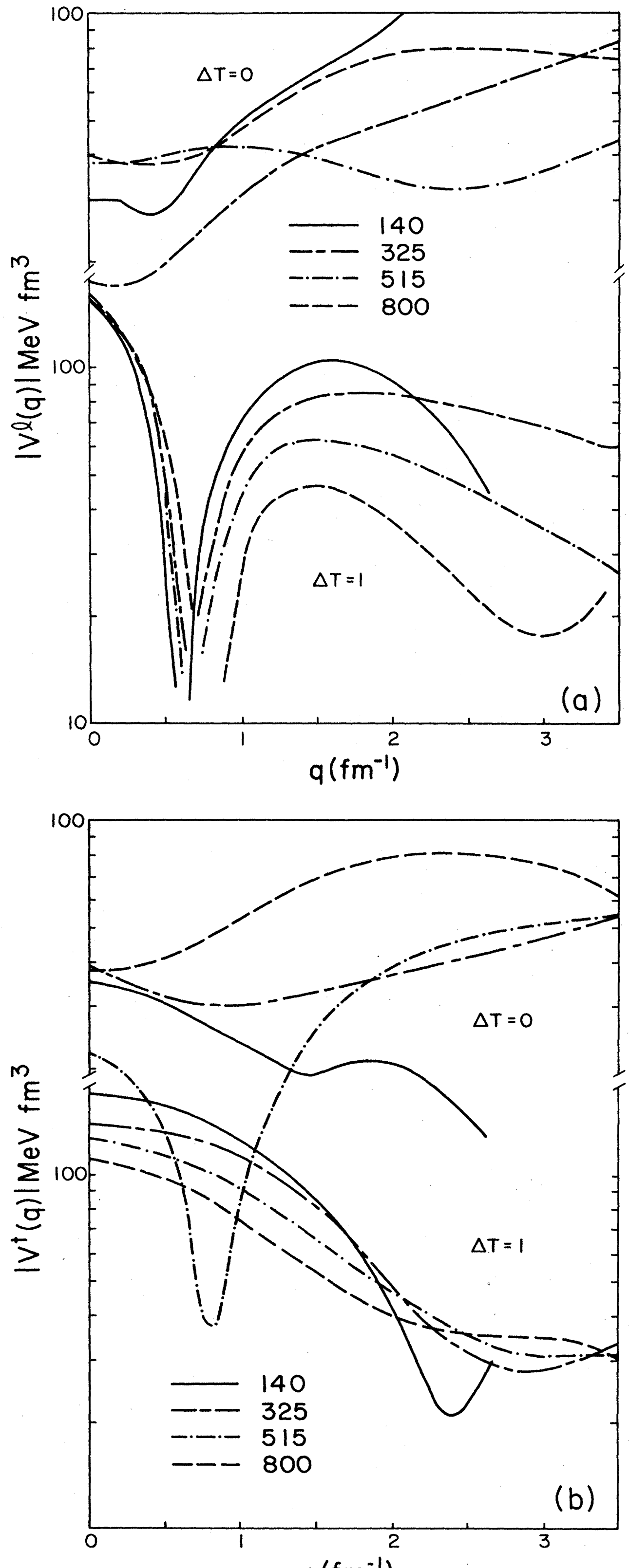

FIG. 3. Energy, momentum transfer, and isospin transfer dependence of the longitudinal and transverse parts of the NN interaction.

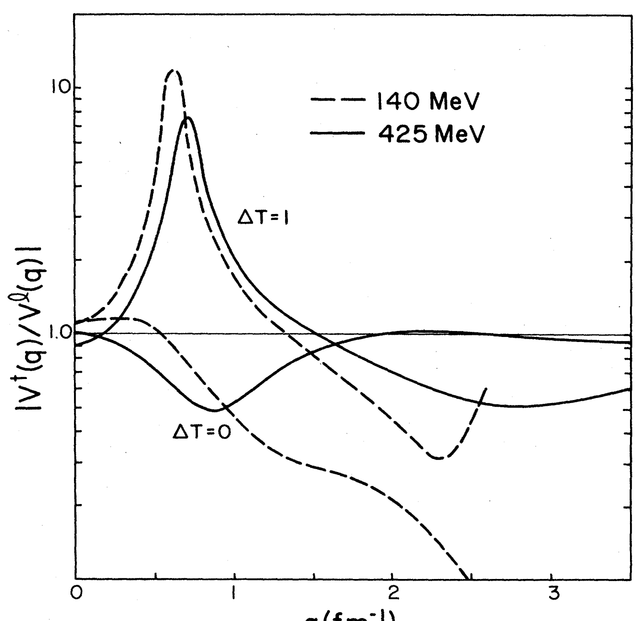

FIG. 4. Modulus of the ratio of transverse to longitudinal NN coupling versus momentum transfer at nucleon energies of 140 and 425 MeV.

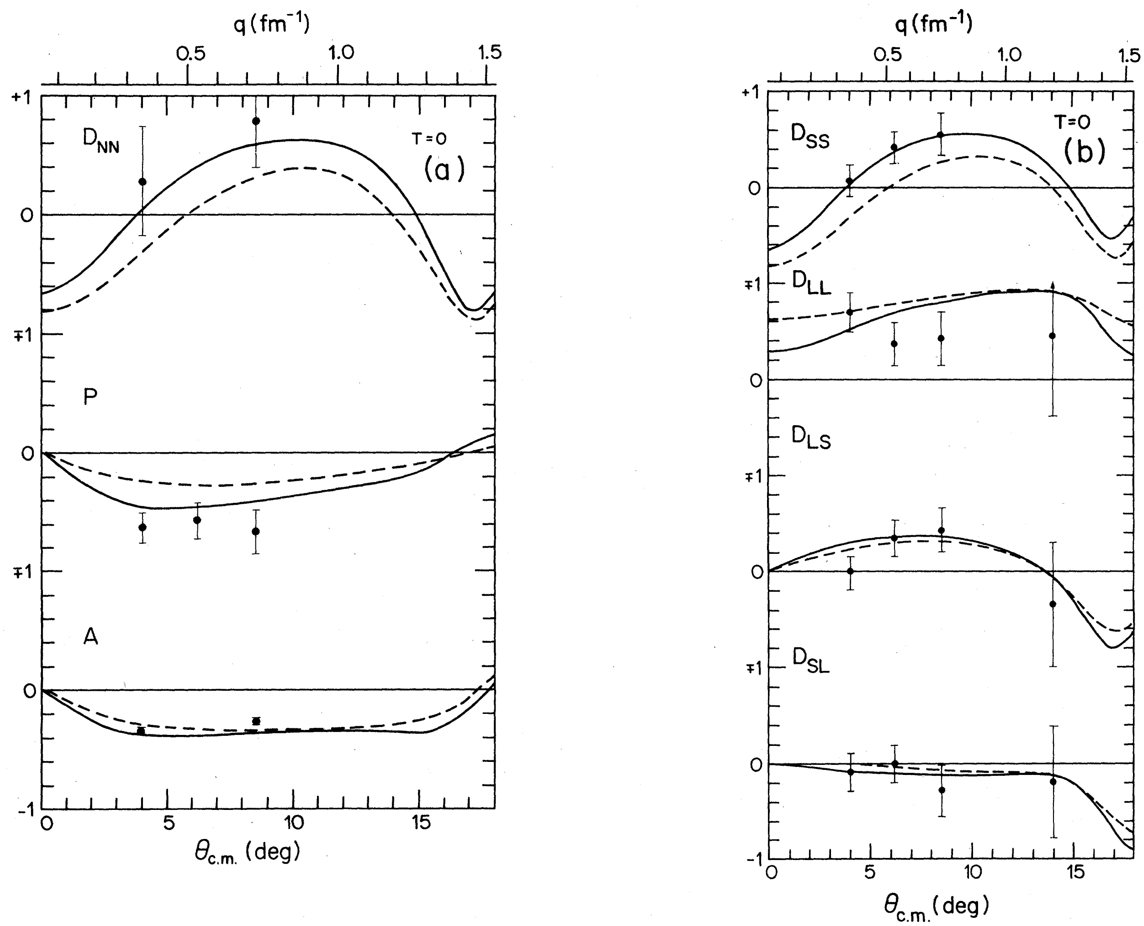

FIG. 5. Comparison between experimental and calculated spin observables at 500 MeV using the present interaction (solid curve) and that given in Ref. 5 (dashed curve). The details are given in the text.

excitations of unnatural parity one should find a close correspondence between (p,p′) and either (e,e′) or (π,π') at small momentum transfer ($q<1.5$ fm^{-1}) where the NN spin coupling is largely transverse. Similarly, a close correspondence amongst these reactions should be found for natural parity spin excitations where only the transverse spin couplings enter.[16] Beyond $q\sim1.5$ fm^{-1} the NN spin coupling is predominantly longitudinal so that the (p,p′) and (p,n) reactions should preferentially excite longitudinal spin modes. This longitudinal dominance of the NN coupling at large momentum transfers is complementary to the purely transverse e-N and π-N spin couplings,[1] and this limits the validity of making direct comparisons between the (p,p′) reaction and either the (e,e′) or (π,π') reaction at these larger momentum transfers. To the extent that high-spin states[1,16] may be described by a single stretched configuration,[19] this uncertainty is removed since the longitudinal and transverse responses are proportional in this case.

Because of their domination by particle interchange (antisymmetrization) and their irregular variation with energy, we regard the isoscalar spin couplings as less reliable than their isovector counterparts. Nevertheless, Fig. 4 suggests a strong dominance of the isoscalar longitudinal coupling near 140 MeV for momentum transfers greater than ~1 fm^{-1}. As in the isovector case this introduces an uncertainty in relating the excitation of unnatural parity states by (p,p′) scattering to that by (π,π') scattering. Insofar as this estimate of the isoscalar longitudinal dominance is reliable, the (p,p′) reaction may be used to probe longitudinal spin excitations which are inaccessible to (e,e′) and (π,π') scattering.

III. APPLICATIONS

It is impractical either to study in detail the differences between the present interaction (Table I) and that in Ref. 5 or to make extensive comparisons with experimental data. We have, however, made a limited number of comparative calculations for a variety of transitions in ^{12}C, ^{28}Si, ^{58}Ni, ^{90}Zr, and ^{208}Pb in the energy range 120–800 MeV. We find, as is suggested by comparing the moments of the interactions, that the two interactions are qualitatively very similar for most types of transitions. An important exception occurs for the excitation of the isobaric analog of the ground state of ^{90}Zr in the ^{90}Zr(p,n) reaction at 200 MeV, where the calculated *peak* cross section is 34% smaller and in better agreement with the data

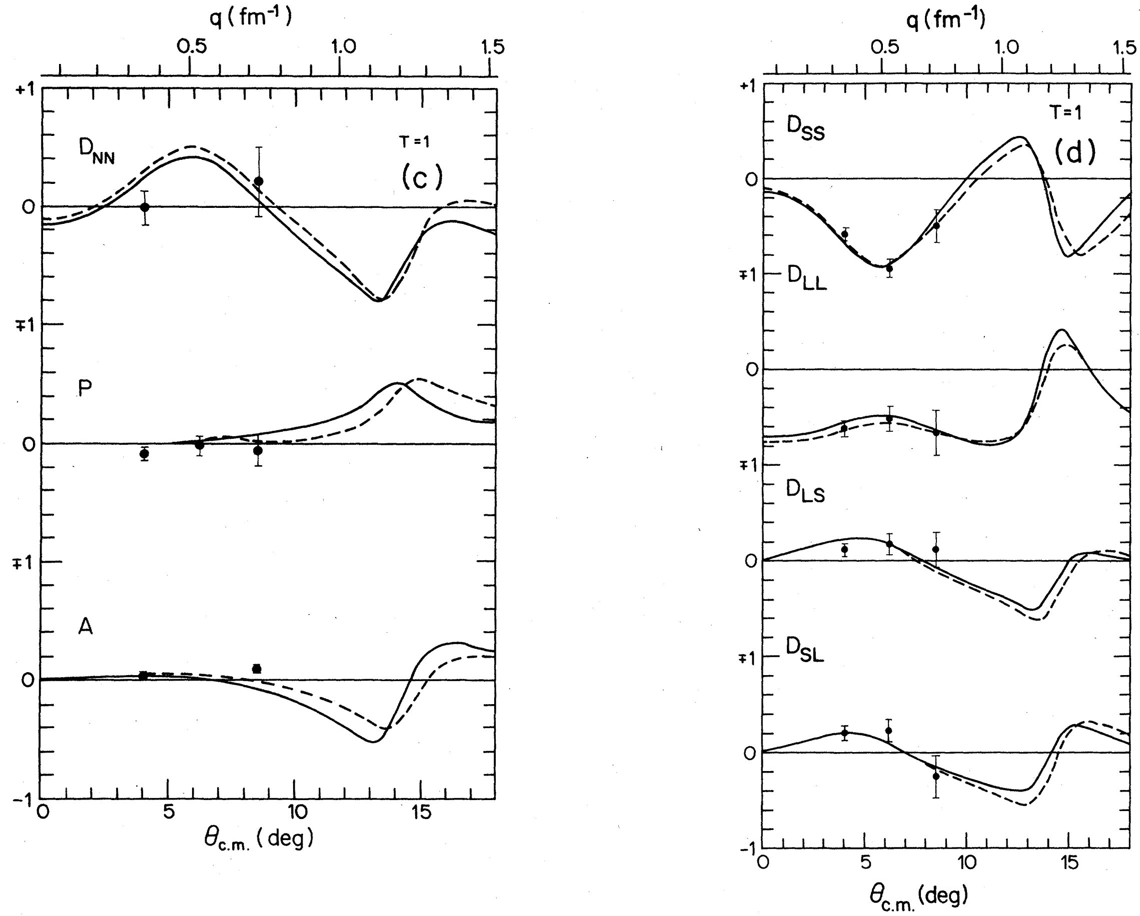

FIG. 5. *(Continued).*

than that obtained using the older interaction.[5] Figure 2 suggests that large differences for this type of reaction may occur over a large energy range. More typically the changes in calculated peak cross sections are $\pm 5\%$. Apart from the isobaric analog transition in ^{90}Zr, the largest differences have been observed near 500 MeV, where there are considerably more NN data than were available when the interaction in Ref. 5 was developed.

As might be expected, the percentage changes in calculated spin observables are somewhat larger than those for the peak differential cross sections. For example, typical changes in calculated analyzing powers near the peak cross sections are $\pm 15\%$, with smaller changes occurring for collective states especially near 200 and 800 MeV. The elastic spin rotation parameters Q (Ref. 20) calculated with the two interactions are quite similar between 200 and 800 MeV so that this new interaction does not resolve the celebrated difficulty[20] in describing Q within a traditional nonrelativistic approach. Since one of the primary motivations for updating the interaction in Ref. 5 is the availability of much more NN and nucleon-nucleus data on spin observables, we show in Fig. 5 a comparison between distorted wave calculations using the previous and the current 515 MeV interactions and the measured[17] spin observables for the excitation of the $T=0$ and $T=1, 1^+$ states in ^{12}C at a proton energy of 500 MeV. The Cohen-Kurath wave functions[21] were used and the optical potential was calculated using the corresponding t-matrix interaction by folding it with the ground state nucleon point density. For the $T=1$ excitation, the differences between the two calculations are rather small and each interaction provides a reasonable description of the spin observables. For the $T=0$ excitation, the differences between the two calculations are larger with the calculation based on the more current SP84 amplitudes being in much better agreement with the data.

IV. SUMMARY

We have presented an updated free t-matrix interaction based on the SP84 amplitudes[12] of Arndt and Roper which, apart from known medium corrections in some NN channels, is tailored for calculations of nucleon-nucleus scattering between 50 and 1000 MeV using nonrelativistic dynamics and relativistic kinematics. The gross properties of this newer interaction are qualitatively similar to those of the interaction given in Ref. 5. Because of this similarity we have illustrated some properties of the newer interaction, such as its longitudinal and transverse components, which are complementary to those illustrated in Ref. 5. Significant differences between the present interaction and that of Ref. 5 do exist and these differences have been found to be most important for calculating spin observables near 500 MeV where much more complete NN data are now available. This is especially true for $T=0$ excitations. Some of the relatively small parts of the interaction such as t_τ have also changed significantly.

ACKNOWLEDGMENTS

We thank R. Arndt for helpful discussions and for permission to use the unpublished SP84 NN amplitudes. This work was supported in part by NSF grants PHY-8206661 and PHY-8441893 and by DOE grant DE-AC02-77ER04215,A007.

[1]F. Petrovich and W. G. Love, Nucl. Phys. **A354**, 499c (1981).

[2]G. Bertsch, Comments Nucl. Part. Phys. **10**, 91 (1981); C. D. Goodman, *ibid.* **10**, 117 (1981).

[3]N. Anantaraman *et al.*, Phys. Rev. Lett. **46**, 1318 (1981).

[4]C. Olmer *et al.*, Phys. Rev. C **29**, 361 (1984).

[5]W. G. Love and M. A. Franey, Phys. Rev. C **24**, 1073 (1981); Phys. Rev. C **27**, 438(E) (1983).

[6]J. R. Comfort *et al.*, Phys. Rev. C **21**, 2147 (1980).

[7]J. Kelly *et al.*, Phys. Rev. Lett. **45**, 2012 (1980).

[8]H. V. von Geramb and K. Nakano, in *Interaction Between Medium Energy Nucleons in Nuclei*—1982, Proceedings of the Workshop on the Interaction Between Medium Energy Nucleons in Nuclei, AIP Conf. Proc. No. 97, edited by H. O. Meyer (AIP, New York, 1983), p. 44.

[9]L. Ray, see Ref. 8, p. 121.

[10]W. Bauhoff *et al.*, Nucl. Phys. **A410**, 180 (1983).

[11]M. V. Hynes, A. Picklesimer, P. C. Tandy, and R. M. Thaler, Phys. Rev. Lett. **52**, 978 (1984).

[12]R. A. Arndt *et al.*, Phys. Rev. D **28**, 97 (1983); R. A. Arndt and L. D. Roper (unpublished).

[13]D. V. Bugg *et al.*, Phys. Rev. C **21**, 1004 (1980).

[14]A. M. Bernstein, V. R. Brown, and V. A. Madsen, Comments Nucl. Part. Phys. **11**, 203 (1983); M. M. Gazzaly *et al.*, Phys. Rev. C **25**, 408 (1982); J. A. Carr, F. Petrovich, and J. J. Kelly (unpublished).

[15]T. N. Taddeucci *et al.*, Phys. Rev. C **25**, 1094 (1981); C. Gaarde *et al.*, Nucl. Phys. **A369**, 258 (1981).

[16]W. G. Love, M. A. Franey, and F. Petrovich, in *Proceedings of the International Conference on Spin Excitations, Telluride, Colorado, 1982,* edited by F. Petrovich, G. E. Brown, G. Garvey, C. D. Goodman, R. A. Lindgren, and W. G. Love (Plenum, New York, 1984), p. 205.

[17]E. Bleszynski, M. Bleszynski, and C. A. Whitten, Jr., Phys. Rev. C **26**, 2063 (1982); J. B. McClelland *et al.*, Phys. Rev. Lett. **52**, 98 (1984).

[18]W. G. Love and G. R. Satchler, Nucl. Phys. **A159**, 1 (1970).

[19]R. A. Lindgren *et al.*, Phys. Rev. Lett. **42**, 1524 (1979).

[20]G. W. Hoffmann *et al.*, Phys. Rev. Lett. **47**, 1436 (1981); B. C. Clark, R. L. Mercer, and P. Schwandt, Phys. Lett. **122B**, 211 (1983).

[21]S. Cohen and D. Kurath, Nucl. Phys. **73**, 1 (1965).